

Model Fitting on Noisy Images from an Acoustofluidic Micro-Cavity for Particle Density Measurement

Lucas M. Massa¹, Tiago F. Vieira¹ ^a, Allan de M. Martins² ^b, Ícaro B. Q. de Araújo¹ ^c,
Glauber T. Silva³ and Harrisson D. A. Santos³

¹Institute of Computing, Federal University of Alagoas, Lourival Melo Mota Av., Maceió, Brazil

²Department of Electrical Engineering, Federal University of Rio Grande do Norte, Natal, Brazil

³Physics Institute, Federal University of Alagoas, Maceió, Brazil

Keywords: Particle Density Estimation, Genetic Algorithm, Gradient Descent, 2D Gaussian Fitting, Acoustofluidics.

Abstract: We use a 3D printed device to measure the density of a micro-particle with acoustofluidics, which consists in using sound waves to trap particles in free space. Initially, the particle is trapped in the microscope's focal plane (no blur). Then the transducers are shut off and the particle falls inside the fluid, increasing its diameter due to defocus caused by the distance to the lens. This increase in diameter along time provides its velocity, which can, in turn, be used to compute its density. To manually annotate the diameter in the recorded images is a tedious task and is prone to errors. That happens due to the high noise present in the images, specially in the last frames where the defocus is high. Because of that, we use a 2D Gaussian model fitting process to estimate the particle diameter throughout different depth frames. To find the diameters, we initially perform the Gaussian parameters fit with Genetic Algorithm in each frame of the recorded particle trajectory to avoid local minima. Then we refine the fit with Gradient Descent using Tensorflow in order to compensate for any randomness present in the fit of the Genetic Algorithm. We validate the method by retrieving a known particle's density with acceptable performance.

1 INTRODUCTION

Separating particles of interest from complex mixtures is an important procedure done in many fields such as biology (Fan et al., 2022) and medicine (Li et al., 2015). Recently, acoustofluidic, which consists in using sound waves propagating through some fluid medium, has been used in areas like clinical diagnostics (Wang et al., 2021) and therapeutics (Bose et al., 2015) due to its capability of trapping particles having specific physical characteristics. By observing isolated particles or conglomerates (colloids), one can confirm the occurrence of specific reactions and determine whether a given pathogen is present in a body fluid sample using a microscope, for instance.

Traditionally, several techniques have been used to separate particles, such as those based on centrifuges, which is time-consuming, can cause substantial material loss and alter cell functions (Fan et al., 2022). In contrast, with a carefully designed acous-

tic field, one can separate target cells embedded in a complex liquid, which has been validated as a viable, contact-less, bio-compatible and label-free technol-

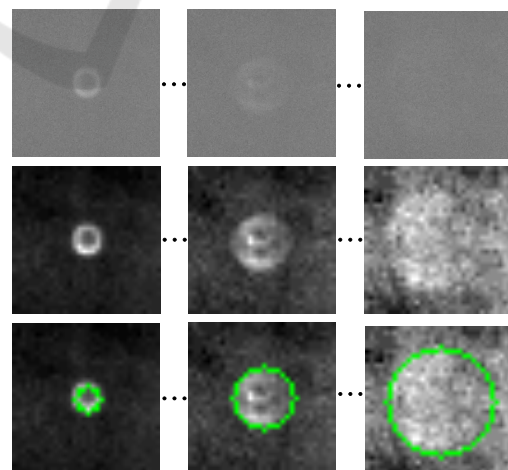


Figure 1: Captured images of a falling particle. The blur gradually increases along the process. First row: original images captured by a microscope. Middle row: Same images with enhanced contrast. Last row: particles fitted by a curve.

^a  <https://orcid.org/0000-0002-5202-2477>

^b  <https://orcid.org/0000-0002-9486-4509>

^c  <https://orcid.org/0000-0002-6769-4946>

ogy. Additionally, by incorporating automation and tackling limitations of conventional strategies, isolating sub-micron bio-particles can potentially accelerate the development of Point-of-Care devices.

In this work, we use an acoustofluidic 3D printed device (fluid chamber) to measure the density of polystyrene beads. The device is initially filled with a fluid in which the analytes are embedded. Transducers are then excited to generate an acoustic field responsible for “trapping” the particle in a given position. A microscope is used to acquire images of the cells as exemplified in Fig. 1, where the “trapped” particle is represented by the first image (top-left). After the acoustic field is disabled, the particle falls along time, causing a strong blur as shown in the middle and final images in Fig. 1, since the particle is no longer within the microscope focus plane. By observing the fall velocity (depth per moment in time) and using a calibration curve obtained in beforehand that relates the particle’s diameter to depth, one can compute a good estimate of the cell’s density (*cf.*, Section 2).

Unfortunately, annotating cell’s diameters on different images is a manual process due to a very low Signal-to-Noise Ratio (SNR) inherent to the blurring process caused by the particle fall and short Depth-of-Field of the microscope optical apparatus. Therefore, one must manually annotate each image in both stages of calibration and dynamic measurement. Manually annotating images is a time-consuming and cumbersome process due to many characteristics. It is prone to human error and fatigue, rendering automation and development of Point-of-Care devices unfeasible.

The bead’s diameter is related to the depth, which can provide information regarding the velocity of the fall (depth per time). It can be shown that the velocity with which the particle falls into the medium, along with other quantities can provide the particle’s density value (*cf.* Section 2). Therefore, we propose a method capable of measuring the particle’s diameters during its fall. Due to the amount of noise, we found that fitting a 2D Gaussian in a Gradient Descent fashion can provide reasonable performance in the final density measurement.

Fitting a Gaussian onto a signal (image) is a method that can be applied on different scenarios for different purposes. For instance, Ananthanarasimhan et al., used the technique to estimate the diameter of discharges viewed by High Speed Cameras (HSC) to characterize a rotating gliding arc (RGA) reactor (Ananthanarasimhan et al., 2022). Kizel et al. proposed a method for fully constrained spatially adaptive spectral unmixing for the localization of endmembers (Kizel et al., 2015). Lei et al., used a 2D Gaussian fitting procedure to lo-

cate motion-blurred, weak celestial objects in images (Lei et al., 2016) for the purpose of orbital debris monitoring. Dai et al., used the method to estimate the Point Spread Functions of different optical apparatus and ultimately increase the resolution of Single-Photon Emission Computerized Tomography (SPECT) to sub-millimeter range (Dai et al., 2010). Anniballe and Bonafoni proposed a Gaussian fitting procedure aimed at analyzing remotely sensed thermal multi-resolution images to monitor variations in urban occupancy throughout area and time (Anniballe and Bonafoni, 2015). Bui et al., proposed the segmentation of murine tumor from noisy ultrasound clinical images using Gaussian distribution to model local intensities (Bui et al., 2015).

In this context, we propose a Computer Vision strategy capable of automatically measuring cell diameter on noisy images using a simple, yet effective, method based on 2D Gaussian fitting using Genetic Algorithm (GA) and a subsequent refinement with Gradient Descent (GD) method. Experiments showed that the methodology provides a satisfactory performance and can eventually contribute to the development of fully automated devices.

2 EXPERIMENTAL METHODOLOGY

The density of a particle embedded in a liquid affects the rate in which it falls (in distance per time). The relation between fall rate and density can be found by analyzing the problem’s dynamics, which, for a particle embedded in a fluidic medium, is ruled by a specific set of forces. As explained by (Zhao et al., 2014), forces caused by particle-to-particle interaction, thermal effects and Brownian motion can be disregarded due to their low order of magnitude when compared with other forces that act on the system. Thus, the resulting force that pulls the particle down along the vertical axis can be expressed as a combination of gravitational, viscosity and buoyancy forces:

$$\sum \vec{F} = \vec{F}_{gravitational} + \vec{F}_{viscosity} + \vec{F}_{buoyancy} \quad (1)$$

Considering that the vertical axis is pointed downward and approximating the particle as a perfect sphere, one can express the forces mentioned above as

$$\vec{F}_{gravitational} = \left(\frac{4}{3} \pi g r^3 \rho_{particle} \right) \hat{k} \quad (2)$$

$$\vec{F}_{buoyancy} = \left(-\frac{4}{3} \pi g r^3 \rho_{fluid} \right) \hat{k} \quad (3)$$

$$\vec{F}_{viscosity} = (6\pi r \mu v) \hat{k}, \quad (4)$$

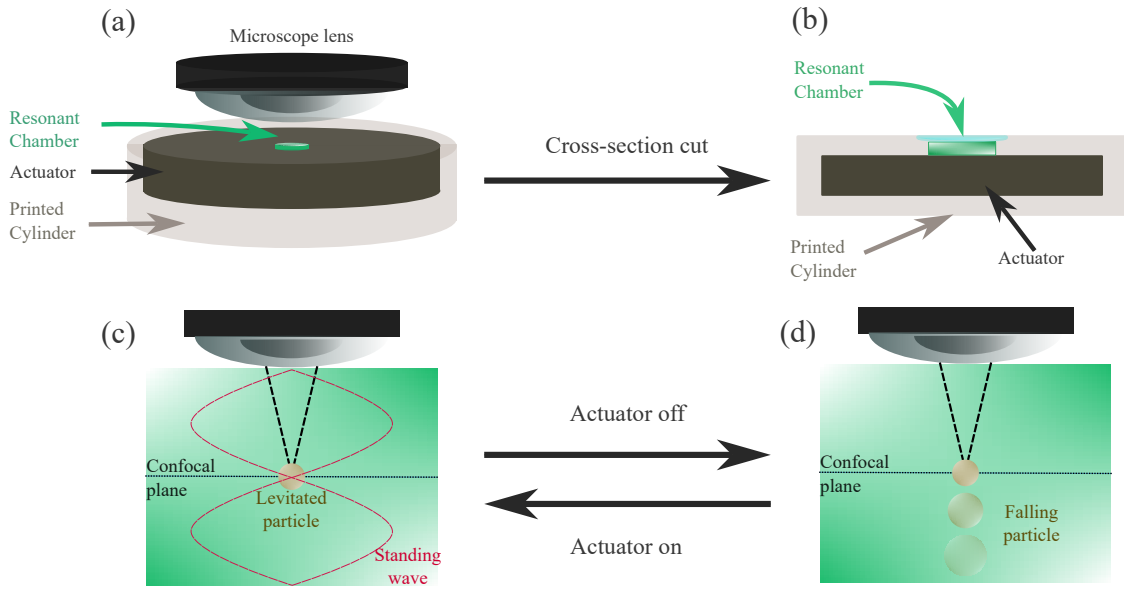


Figure 2: (a) Diagram of the used hardware. (b) Cross-section cut illustration of the device shown in (a). (c) When the actuator is on, a standing wave is generated and the particle is trapped in the microscope confocal plane. (d) When the actuator is turned off, the wave vanishes and the particle falls downwards presenting what we call a *dynamic* behaviour.

where $\rho_{particle}$ is the particle's density, ρ_{fluid} is the fluidic medium's density, r is the sphere's radius, μ is the fluid's dynamic viscosity and v is the particle's velocity during fall.

Therefore, by applying Newton's second law, considering v as particle's velocity along z axis and solving the resulting differential equation for the intensities of the forces defined above, the following expression is found (Zhao et al., 2014):

$$v(t) = \frac{2r^2g(\rho_{particle} - \rho_{fluid})}{9\mu}(1 - e^{-\frac{t}{\tau}}) \quad (5)$$

Since $\tau = m/6\pi r\eta K$ is very small, the exponential term from Equation (5) can be ignored. Manipulating the resulting expression, one can find the final relation between particle density and fall velocity:

$$\rho_{particle} = \frac{9\mu v}{2r^2g} + \rho_{fluid}. \quad (6)$$

I.e., one can compute the particle's density (in kilograms per cubic meters) if its fall velocity and its radius are known. During the course of this work we will analyze the dynamics of $10\mu\text{m}$ diameter polystyrene beads, which have a well known density of around $1050 \text{ kg}\cdot\text{m}^{-3}$.

2.1 Hardware

For the acoustofluidic device, a cylindrical structure was fabricated using a 3D printer (*cf.*, Fig. 2a) (Santos et al., 2021). A small disk with a diameter of 4mm

and a height of $750\mu\text{m}$ was cast inside the cylindrical structure and top sealed by a glass cover which also acted as an acoustic reflector (*cf.*, Fig. 2b). This disk was used as a resonant chamber inside which particles were placed. A small inlet hole could be used to fill the chamber with fluid solutions of particles. This solutions could later be removed by an outlet hole. To deliver our experiments we used a fluidic solution with density and dynamic viscosity values of $997 \text{ kg}\cdot\text{m}^{-3}$ and $0.89 \times 10^{-3} \text{ Pa}\cdot\text{s}$, respectively. At the bottom of the acoustic chamber a circular piezoelectric actuator, with a diameter of 25mm , was attached. When the actuator is turned on, an acoustic standing wave is produced inside the resonant chamber (*cf.*, Fig. 2c). This creates an acoustic radiation force that traps the particles in a standing wave node, which has a height of approximately $95 \times 10^{-6} \text{ m}$ from chamber's bottom. An optical microscope is placed above the cylindrical structure such that confocal plane matches the wave node where particles are levitated. Turning off the actuator causes the acoustic forces to be extinguished (*cf.*, Fig. 2d), so the particles fall within the fluidic medium. As the particles fall, they gradually move away from microscope's confocal plane, becoming increasingly blurry in acquired images.

2.2 Pipeline for Single Particle Configuration

During the course of this work, the fluidic solutions introduced inside the acoustic chamber generally con-

tained around 100 particles. A particle-to-particle interaction caused the appearance of grouped packs of particles, which makes it difficult to carry out the experiments. To achieve a single-particle configuration, a sequence of two steps was carefully followed. Firstly, once a pack of particles started to emerge, the actuator power was turned off. Lastly, about 10 seconds later, the device was turned on again, causing only a single particle to be trapped at the acoustic wave pressure node. Through this pipeline the proposed experiments could be successfully conducted.

2.3 Calibration

As it was already discussed, the density of a particle can be measured by a model based on the fall process inside a microfluidic cavity along with a confocal optical inspection. As the particle falls, the relative distance to the image confocal plane becomes larger. This results in a blurring effect, which increases the particle size in the image as it gets increasingly defocused.

To analyze the dynamics of a particle with a specific diameter and unknown density, it is necessary to use a calibration curve that relates the relative area of a particle, which has the same diameter, with previously known heights between particle and the resonant cavity bottom during a fall process, as shown in Fig. 4. Considering that we have n (in our experiments we used 18 images for the calibration step) acquired images from a particle during fall and its respective heights and areas, relative area values can be computed by the following equation:

$$A_{relative} = \frac{A_i - A_1}{A_n - A_1} \quad (7)$$

where A_1 , A_i and A_n are, respectively, area values for the first, current and last captured images.

Therefore, the computed values for relative area and height can be fitted to a double exponential function, which is defined as follows:

$$h = \alpha_1 \exp\left[-\frac{A_{relative}}{\beta_1}\right] + \alpha_2 \exp\left[-\frac{A_{relative}}{\beta_2}\right] + \omega_0 \quad (8)$$

where α_1 , α_2 , β_1 , β_2 and ω_0 can assume arbitrary values, having no physical meaning. The resulting curve can be later used to estimate height values for a new particle by applying as input the relative area values during a fall experiment. Lastly, we can derive the obtained height values to estimate the falling velocity for that particle and with Eq. (6), find its density.

2.4 Curve Fitting

An important aspect of the particle area measurement process is that it is done manually, being more susceptible to errors. This problem could be overcome through the usage of a procedure to automatically compute the particle area in the captured image. Aiming to achieve such solution, during this step we investigated the feasibility of fitting well known curves to the particle area in an input image. The tests focused mainly in the application of 2D Gaussian functions for this task. The Gaussian is given by the following expression:

$$z(x,y) = p \exp\left[-\left(\frac{(x-\mu_x)^2}{2\sigma^2} + \frac{(y-\mu_y)^2}{2\sigma^2}\right)\right] \quad (9)$$

where:

- p : Gaussian amplitude.
- μ_x : Position of the Gaussians center in the image along the (horizontal) x-axis.
- μ_y : Position of the Gaussians center in the image along the (vertical) y-axis.
- σ : Standard deviation of the Gaussian (proportional to the radius of the image)

The idea is to fit the Gaussian model into the image by minimizing the mean square error (MSE) between the Gaussian and each pixel in the image. This technique is very powerful provided that the noise is symmetric. Regardless of the amplitude of the noise present in the image the model will have minimum MSE only when the parameters of the Gaussian fit as best as possible with the object in the image.

Once fitted, the Gaussian parameters can be used to give us measures on the object like its position (mean of the Gaussian) and size (standard deviation).

2.5 Genetic Algorithm

Defining a Gaussian function that fits to the particle in an input image is not trivial. From Eq. (9), we can consider p , μ_x , μ_y and σ^2 as curve parameters. Hence, the task of finding values that best fits a specific particle image becomes a non-convex optimization problem.

A common approach to perform optimization tasks in such cases is the usage of Genetic Algorithms (GA). This kind of algorithms are inspired by evolutionist theory, where natural selection keeps alive only the individuals that are more adapted to the environment and give them the opportunity to pass their genes to future generations. As exposed by (Konak et al.,

2006), in the GA formalism each individual is represented by a vector called *chromosome*. Chromosomes vectors are formed by values called *genes*. Each chromosome is considered to be a solution to the problem which is being optimized and are grouped in a set called *population*. The chromosome vectors generally are randomly initialized and through the combination of their genes, in a iterative process, converge to an optimized solution.

During this iterative process, two main operations are conducted: *crossover* and *mutation*. Firstly, in the crossover operation, two chromosomes combine their genes to generate a new one. Lastly the mutation introduces the chance of random changes to the genes, which also happen in nature. At each iteration only the most adapted individuals are used to perform the crossover operation. This metric of how much an individual is adapted to the problem is called *fitness* and is calculated through a function that is defined according to the optimization problem necessities.

Hence, we tested a Genetic Algorithm approach for the Gaussian function optimization. The population was formed by chromosomes with the format $[p, \sigma^2]$, which are parameters used to generate Gaussian curves, as denoted by Eq. 9. During this step we utilized 13 images of a single particle which were acquired consecutively during the fall process. The particle initially appears clear and focused and gradually blurs along the sequence of images. The following preprocessing steps were done:

- Aligning the particle at the center of the image.
- Image resizing to a 32×32 shape.
- Subtraction of a mean background value.

Then, the resulting images were applied to the genetic algorithm parameter optimization, which intended to find the best p and σ^2 values for a 2D Gaussian function. As the particles were centralized by the pre-processing steps, we fixed the μ_x and μ_y parameters to zero. The genetic algorithm was executed for 1000 generations, 100 individuals and a mutation rate of 1%. The fitness of each individual was measured by the Mean Squared Error between the processed image and the Gaussian curve created with the current parameter values. This process was repeated for each test image generating 13 sets of optimized p and σ^2 values.

2.6 Model Fitting Using Gradient Descent Method

As the genetic algorithm is not deterministic, it may not reach the global minimum of the error function.

Thus, a natural step is to apply a more controlled optimization method having as a starting point the best parameters found for each image by the approach described at Section 2.5. For this task we tested the application of a Stochastic Gradient Descent (Bottou, 2012) optimizer for p and σ^2 parameters.

Considering that we have a particle image y and we want to approximate it by a Gaussian curve $z(p, \sigma^2)$, our goal is to find p and σ^2 values that minimize a chosen loss function $L(z(p, \sigma^2), y)$, which evaluates how far the generated curve is from the desired one. Differential calculus defines the gradient of a function as a vector that indicates the direction to move from the current input parameters point so that one can get the greatest increase rate. Thus, one can minimize the function value by moving to the opposite direction, which is called *gradient descent*.

Therefore, assuming $w = [p, \sigma^2]$ as an input vector, we can minimize the loss by updating it's values in a iterative process by using the following expression

$$w_{i+1} = w_i - \alpha \nabla_w L(z(w), y) \quad (10)$$

where α is called learning rate and is responsible for determining the update step size at each iteration.

Taking into account that the genetic algorithm achieved results close to a global minimum, the curve gradient at this point will have very small values. To tackle this scenario, we used a higher learning rate value of 2.0. We also executed the process for 1000 epochs for each set of test images and initial parameters and applied a Mean Squared Error loss function, which, for two input images, can be defined as follows:

$$MSE = \frac{1}{WH} \sum_{x=0}^{W-1} \sum_{y=0}^{H-1} [f(x, y) - g(x, y)]^2 \quad (11)$$

where W and H are, respectively, images' width and height values.

3 RESULTS AND DISCUSSION

3.1 Height and Relative Area Curve

By applying the proposed methodology, we were able to obtain a calibration curve for the experiment. With the usage of ground-truth images, where particle's contour was previously known, we extracted particle's radius from a pixel-micron relation. Then, we calculated area values by considering the particle as a perfect circle and, along with it's respective height values, we could generate a calibration curve that related particle height with relative area, as discussed in

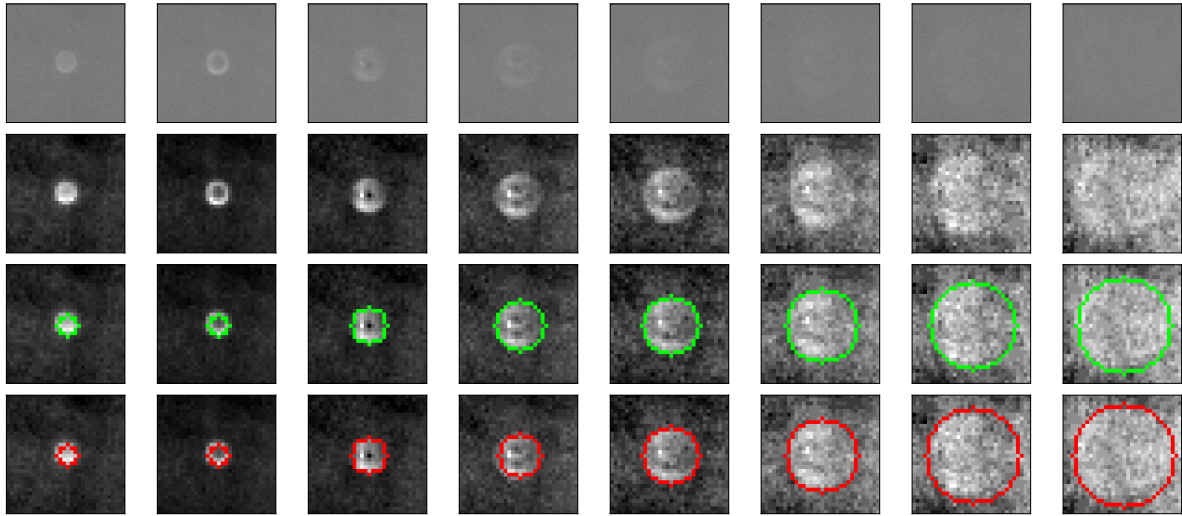


Figure 3: Image grid showing the results for diameter estimation. First row: Original images (last 8 slices from left to right – ie. heights). Second row: Processed images. Third row: Contours obtained with the Genetic Algorithm. Bottom row: Contours found using the Gradient Descent approach.

section 2.3. Numerically fitting the points to the proposed double exponential function (Eq. (8)), we could achieve the curve shown in Fig. 4.

3.2 Genetic Algorithm and Gradient Descent

After the application of the pipeline proposed in Sections 2.5 and 2.6, we could achieve good results for all test images. Figure 3 presents an image grid containing results for eight of the thirteen tested images. Despite being stochastic, the genetic algorithm was able to find good parameters for the 2D Gaussian functions. As shown in the second row of Fig. 3, the contours of resulting Gaussian curves seem to fit, if not perfectly match, the particle contour. The results are even more interesting for the last images of the sequence, where we find a high amount of noise and a

clear contour for the particle is not visually identifiable. Still, the algorithm was able to find plausible parameters for the Gaussian curves as we can see in Fig. 4.

The application of the Stochastic Gradient Descent optimizer did not change the results in general. Despite giving a lower loss value, the resulting Gaussian curve was practically the same. The only exceptions were the results for three of the thirteen test images, which are shown in fourth, seventh and eighth columns of Fig. 3. The optimization produced a visible result, since curve contours changed slightly with respect to the ones found by the genetic algorithm. However, for all other images, the plotted Gaussian contour was exactly the same, which ratifies the good result found by the genetic approach. In Fig. 5 we can see resulting loss curves for the parameter tuning process.

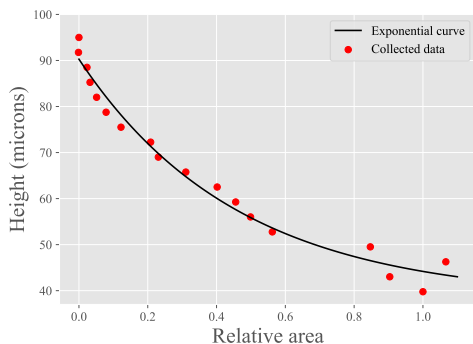


Figure 4: Curve obtained by fitting an exponential function to height and relative area values during the calibration process.

3.3 Density Measurement

Lastly, we used the obtained Gaussian curves to compute particles' areas in each image and generate relative area values by applying Eq. (7). Such values could then be used as input for the calibration curve discussed in Sections 2.3 and 3.1 to estimate particle's height at each image, which are shown in Figure 6.

Then, we numerically derived the height curve and applied the mean value as particle's velocity in Eq. (6) to compute the particle's density. For this computation we also used a gravitational acceleration of $g = 9.82 \text{ m}\cdot\text{s}^{-2}$ along with previously discussed values of $\rho_{fluid} = 997 \text{ kg}\cdot\text{m}^{-3}$ and $\mu = 0.89 \times$

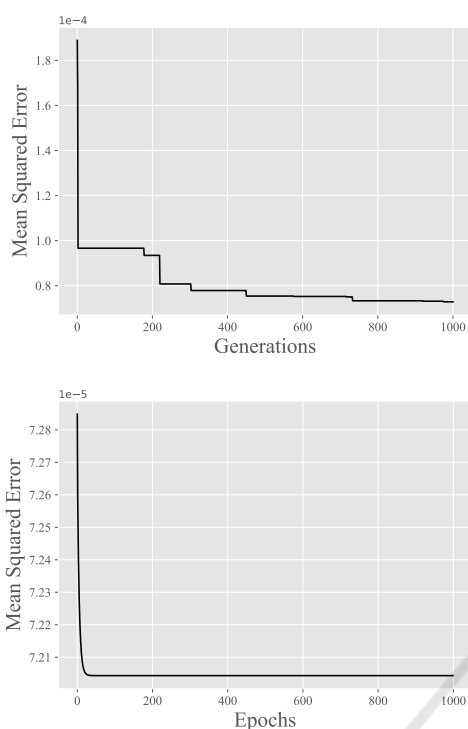


Figure 5: Example loss curves during the parameter optimization process. Plots show, respectively, results for genetic algorithm and gradient descent steps.

10^{-1} Pa·s. This procedure resulted in a density value of $1059 \text{ kg}\cdot\text{m}^{-3}$, which is close to the real density value of $1050 \text{ kg}\cdot\text{m}^{-3}$, corresponding to an error of 0.8%.

Such result ratifies our approach as a valid mean to estimate the area of a particle and its density by applying the previously described equations. It is worth mentioning that even in extreme cases, where the particle was not easily identifiable and the image contained a lot of noise, the proposed method was capable of giving good estimates for Gaussian curve approximation for the particle, consequently allowing the computation of its density.

4 CONCLUSIONS

We presented a methodology to obtain a sub-micron particle's density using acoustofluidics. This approach is traditionally performed manually, which renders the development of point-of-care devices unfeasible.

Aiming at automating the process, we proposed the use of 2D Gaussian fitting to retrieve particle's diameters throughout different positions during fall as an alternative to analyze its velocity and compute its

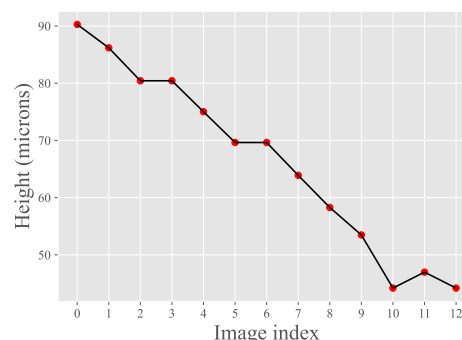


Figure 6: Estimated height for each image by applying computed Gaussian areas as input to the calibration curve.

density. After a calibration procedure, the fall dynamics was analyzed and the diameters were used as inputs to the calibration function in order to obtain the corresponding depths along time. This fall velocity is used alongside different parameters in a given formulation to compute the density. Given a reference known value of $1050 \text{ kg}\cdot\text{m}^{-3}$ the method provided a value of $1059 \text{ kg}\cdot\text{m}^{-3}$, satisfactorily close to the calibration density. As future work, we intend to analyze the usage of blur score metrics related to Gradient, Laplacian, Fourier Transform and wavelets as an approach to the discussed particle fitting problem.

ACKNOWLEDGEMENTS

This work was partially funded by SOFTEX¹.

REFERENCES

- Ananthanarasimhan, J., Raghuram, A., and Rao, L. (2022). Arc diameter estimation of a rotating gliding arc using a simple highspeed camera and gaussian fit function. *IEEE Transactions on Plasma Science*, 50(6):1401–1406.
- Anniballe, R. and Bonafoni, S. (2015). A stable gaussian fitting procedure for the parameterization of remote sensed thermal images. *Algorithms*, 8(2):82–91.
- Bose, N., Zhang, X., Maiti, T. K., and Chakraborty, S. (2015). The role of acoustofluidics in targeted drug delivery. *Biomicrofluidics*, 9:052609.
- Bottou, L. (2012). Stochastic gradient descent tricks. In *Neural networks: Tricks of the trade*, pages 421–436. Springer.
- Bui, T. M., Coron, A., Mamou, J., Saegusa-Becroft, E., Machi, J., Dizeux, A., Bridal, S. L., and Feleppa, E. J. (2015). Level-set segmentation of 2d and 3d ultrasound data using local gamma distribution fitting en-

¹<https://softex.br/>

- ergy. In *2015 IEEE 12th International Symposium on Biomedical Imaging (ISBI)*, pages 1110–1113.
- Dai, T., Ma, T., Liu, H., Cui, J., Liu, Y., Wei, Q., Wu, J., Wang, S., and Jin, Y. (2010). Low-cost high-resolution animal spect imaging on a clinical spect scanner. In *2010 3rd International Conference on Biomedical Engineering and Informatics*, volume 1, pages 341–344.
- Fan, Y., Wang, X., Ren, J., Lin, F., and Wu, J. (2022). Recent advances in acoustofluidic separation technology in biology. *Microsystems & Nanoengineering*, 8:94.
- Kizel, F., Shoshany, M., and Netanyahu, N. S. (2015). Spatially adaptive hyperspectral unmixing based on sums of 2d gaussians for modelling endmember fraction surfaces. In *2015 IEEE International Geoscience and Remote Sensing Symposium (IGARSS)*, pages 4440–4443.
- Konak, A., Coit, D. W., and Smith, A. E. (2006). Multi-objective optimization using genetic algorithms: A tutorial. *Reliability engineering & system safety*, 91(9):992–1007.
- Lei, Z., Chen, X., and Lei, T. (2016). Sub-pixel location of motion blurred weak celestial objects in optical sensor image based on elliptical 2d gaussian surface fitting. In *2016 International Conference on Industrial Informatics - Computing Technology, Intelligent Technology, Industrial Information Integration (ICIICII)*, pages 100–104.
- Li, P., Mao, Z., Peng, Z., Zhou, L., Chen, Y., Huang, P.-H., Truica, C. I., Drabick, J. J., El-Deiry, W. S., Dao, M., Suresh, S., and Huang, T. J. (2015). Acoustic separation of circulating tumor cells. *Proceedings of the National Academy of Sciences*, 112:4970–4975.
- Santos, H. D. A., Silva, G. C., Vieira, T. F., Silva, A. E., de Araújo, B. Q., Jacinto, C., Rocha, U., Alexandre-Moreira, M. S., and Silva, G. T. (2021). Measuring cell density in a acoustofluidic microcavity. In *2021 IEEE UFFC Latin America Ultrasonics Symposium (LAUS)*, pages 1–4.
- Wang, Z., Wang, H., Becker, R., Rufo, J., Yang, S., Mace, B. E., Wu, M., Zou, J., Laskowitz, D. T., and Huang, T. J. (2021). Acoustofluidic separation enables early diagnosis of traumatic brain injury based on circulating exosomes. *Microsystems & Nanoengineering*, 7:20.
- Zhao, Y., Lai, H. S. S., Zhang, G., Lee, G.-B., and Li, W. J. (2014). Rapid determination of cell mass and density using digitally controlled electric field in a microfluidic chip. *Lab Chip*, 14:4426–4434.